FDTD and PSTD Simulations for Plasma Applications

Guo-Xin Fan, *Member, IEEE*, Qing Huo Liu, *Senior Member, IEEE*, and Scott A. Hutchinson, *Member, IEEE*

***Abstract*—Three-dimensional finite-difference time-domain (FDTD) and pseudospectral time-domain (PSTD) algorithms, with perfectly matched layer absorbing boundary condition, are presented for nonmagnetized plasma as a special case of general inhomogeneous, dispersive, conductive media. The algorithms are tested for three typical frequency bands, and an excellent agreement between the FDTD/PSTD numerical results and analytical solutions is obtained for all cases. Several applications, such as laser-pulse propagation in plasma hollow channels, surface-wave propagation along a plasma column of finite length, and energy deposition of electron cyclotron resonance plasma source, demonstrate the capability and effectiveness of these algorithms. The PSTD algorithm is more efficient and accurate than the FDTD algorithm, and is suitable for large-scale problems, while the FDTD algorithm is more suitable for fine details. The numerical results also show that plasma has complex transient responses, especially in the low-frequency and resonance regimes. Because of their flexibility and generality, the algorithms and computer programs can be used to simulate various electromagnetic waves-plasma interactions with complex geometry and medium properties, both in time and frequency domains.**

***Index Terms*—Finite-difference time-domain method, perfectly matched layer , plasma, plasma applications, plasma sources, pseudospectral time-domain method.**

I. Introduction

INTERACTION between electromagnetic waves and plasma has been an important research topic. It has found extensive applications in both laboratories and industry, such as ionosphere wave propagation, short-pulse laser-plasma interaction, and microwave excited plasma source for semiconductor processing.

Plasma is a highly frequency-dispersive medium, and its frequency dispersion can significantly change the electromagnetic response in the medium. For an operating frequency lower than ($\omega < \omega_p$), close to ($\omega \sim \omega_p$), and higher than ($\omega > \omega_p$) the plasma frequency ω_p, the electromagnetic fields have drastically different behaviors. In addition, the collision frequency ν_c, another medium parameter, has important effects on the attenuation of waves in plasma. These properties greatly increase the complexities and difficulties of numerical solutions.

Manuscript received April 4, 2000; revised December 22, 2000. This work was supported by Sandia National Laboratories under an SURP Grant, by the Environmental Protection Agency through PECASE Grant CR-825-225-010, and by the National Science Foundation through CAREER Grant ECS-9702195.

G.-X. Fan and Q. H. Liu are with the Department of Electrical and Computer Engineering, Duke University, Durham, NC 27708 USA (e-mail:qhlilu@ee.duke.edu).

S. A. Hutchinson is with Sandia National Laboratories, Albuquerque, NM 87185 USA.

Publisher Item Identifier S 0093-3813(01)02892-2.

In recent years, finite-difference time-domain (FDTD) method, one of the most powerful full-wave computational methods, has been applied to plasma to incorporate the frequency dispersion. Three main classes of algorithms have been proposed: recursive convolutions (RC) [1]–[3]; auxiliary differential equation (ADE) or direct integration (DI) [4]–[6]; and *Z*-transform (ZT) [7]. It is reported that among these methods, the modified version of RC, i.e., the piecewise-linear recursive convolution (PLRC) method, is most accurate and requires the least memory [3], [6].

When simulating an open-region problem, all previous work on FDTD for plasma application employed absorbing boundary conditions (ABCs), such as Mur's [8] and Liao's [9] ABCs, to truncate the computational domain. Despite their success, these ABCs provide only limited absorption to waves within a specific range of incidence angles and frequency. Recently, a highly effective ABC, the perfectly matched layer (PML), was presented, which at the continuum limit, gives zero reflection at the absorbing boundary for all frequency, and all angles of incidence [10]. In addition, the PML is ideal for parallel computation. The PML has been demonstrated to be the most efficient ABC to date, and found intensive applications for various nondispersive and dispersive media when combined with the FDTD method. However, to our knowledge, the PML has not been applied to plasma until very recently [11], [12].

Although the FDTD method has found widespread successful applications, to ensure the accuracy of the computed spatial derivatives of electromagnetic fields, the FDTD method requires a fine spatial discretization of more than 10 cells per minimum wavelength, which limits the scale of problem solvable by FDTD method with the existing computation resources. As one of the improvements, the pseudospectral time-domain (PSTD) algorithm has been recently developed for nondispersive media, and proves to provide high accuracy and efficiency for large-scale problems [13]. This new algorithm was then extended to general dispersive media [12] and for ground-penetrating radar applications in dispersive media [14]. The efficiency of the PSTD method is due to the accurate approximation of spatial derivatives using the fast Fourier transform (FFT). Hence, the spatial sampling rate in the PSTD method approaches the Nyquist sampling rate, i.e., two points per minimum wavelength. A comparative study of the FDTD and PSTD methods for nondispersive media can be found in [13].

In this paper, three-dimensional (3-D) FDTD and PSTD algorithms incorporated with the PML are presented for plasma as a special example of general inhomogeneous, dispersive media. Section II develops the formulation of algorithms,

0093–3813/01$10.00 © 2001 IEEE

and Section III gives several examples for validation and applications.

II. Formulation

A. PML Equations for Dispersive Media

The details of PML formulation for general dispersive media have been developed in [11], [12]. Here, we specialize this formulation to plasma applications.

According to the PML approach [15], all the fields and sources, $\mathbf{E}$, $\mathbf{D}$, $\mathbf{H}$, $\mathbf{J}$, and $\mathbf{M}$, are split in the following forms:

$$\mathbf{E} = \sum_{\eta=x,\,y,\,z} \sum_{\xi\neq\eta} E_{\xi}^{(\eta)}. \tag{1}$$

For an isotropic, conductive, inhomogeneous, linear permittivity dispersive medium, the modified Maxwell's curl equations for the split fields ($\eta = x,\, y,\, z$) in the time domain can be written as [11]

$$\frac{\partial}{\partial\eta}(\hat{\eta}\times\mathbf{E}) = -a_\eta\mu\frac{\partial\mathbf{H}^{(\eta)}}{\partial t} - \mu\omega_\eta\mathbf{H}^{(\eta)} - \mathbf{M}^{(\eta)} \tag{2}$$

$$\frac{\partial}{\partial\eta}(\hat{\eta}\times\mathbf{H}) = a_\eta\frac{\partial\mathbf{D}^{(\eta)}}{\partial t} + \omega_\eta\mathbf{D}^{(\eta)} + a_\eta\sigma\mathbf{E}^{(\eta)} + \omega_\eta\sigma\int_{-\infty}^{t}\mathbf{E}^{(\eta)}\,dt + \mathbf{J}^{(\eta)} \tag{3}$$

where a_η and ω_η correspond to the real and imaginary parts of the complex coordinate stretching variable [16], respectively, and are chosen independent of frequency inside the frequency band of interest. When $a_\eta = 1$ and $\omega_\eta = 0$, the above equations reduce to the conventional Maxwell's equations.

Since both $\mathbf{E}^{(\eta)}$ and $\mathbf{H}^{(\eta)}$ have two scalar components perpendicular to $\hat{\eta}$, and $\mathbf{D}^{(\eta)}$ also has the two corresponding components due to the constitutive relations of the media, Eqs. (2) and (3) consist of a total of 12 scalar equations. These equations are insufficient to solve the total 18 field components. The remaining equations will be given by the constitutive relations as discussed in the next section.

B. Recursive Convolution Approaches

Noting that the constitutive relations take the same form for all split components, we omit all the superscript (η) in this subsection for simplicity.

For a linear dispersive medium, the relationship between the electrical flux density and the electric field intensity in the time domain is described in a convolution integral form as

$$\mathbf{D}(t) = \epsilon_0\epsilon_\infty\mathbf{E}(t) + \epsilon_0\int_{-\infty}^{t}\mathbf{E}(\tau)\chi(t-\tau)\,d\tau \tag{4}$$

where

ϵ_0 free-space permittivity;
ϵ_∞ relative permittivity at $\omega\to\infty$;
χ electric susceptibility.

Equation (4) shows the nonlocal temporal relation between $\mathbf{D}$ and $\mathbf{E}$ for frequency-dispersive media.

Similar to the transfer function of a linear system, the time-domain susceptibility functions for a linear-dispersive medium can be generally expressed as the summation of exponentially damped sinusoids, i.e.,

$$\chi(t) = \sum_{q=1}^{N}\mathrm{Re}[\hat{\chi}_q(t)] = \sum_{q=1}^{N}\mathrm{Re}[R_q e^{s_q t}U(t)] \tag{5}$$

where $U(t)$ is the unit step function, s_q and R_q are the pole and residue, respectively. When s_q and R_q are real, $\hat{\chi}_q$ and all other derived functions below are also real.

To evaluate (4), we introduce a unified linear approximation to $\mathbf{E}(t)$ over the time interval $t\in[m\Delta t,\,(m+1)\Delta t]$ as follows,

$$\mathbf{E}(t) \approx \mathbf{E}(m+1) + K_a\frac{[\mathbf{E}(m+1)-\mathbf{E}(m)]}{\Delta t}\cdot[t-(m+1)\Delta t]. \tag{6}$$

It is noted that (6) corresponds to the recursive convolution (RC) [1] when $K_a = 0$, and to the PLRC [3] when $K_a = 1$.

Using (5) and (6), the convolution integral in (4) is then transformed into the discrete convolution summation

$$\mathbf{D}(n) = \epsilon_0\epsilon_\infty\mathbf{E}(n) + \epsilon_0\sum_{q=1}^{N}\mathrm{Re}[\mathbf{\Psi}_q(n)] \tag{7}$$

where

$$\mathbf{\Psi}_q(n) + \sum_{m=0}^{n-1}\{[\hat{\chi}_q(0)-\hat{\xi}_q(0)]\mathbf{E}(n-m) + \hat{\xi}_q(0)\mathbf{E}(n-m-1)\}e^{s_q m\Delta t} \tag{8}$$

$$\hat{\chi}_q(0) = \begin{cases} R_q\Delta t, & \text{for } s_q = 0 \\ \dfrac{R_q}{s_q}(e^{s_q\Delta t}-1), & \text{for } s_q \neq 0 \end{cases} \tag{9}$$

$$\hat{\xi}_q(0) = \begin{cases} \dfrac{K_a R_q\Delta t}{2}, & \text{for } s_q = 0 \\ \dfrac{K_a R_q}{s_q^2\Delta t}[1-(1-s_q\Delta t)e^{s_q\Delta t}], & \text{for } s_q \neq 0. \end{cases} \tag{10}$$

The above equations, together with the recursion relations for $\mathbf{\Psi}_q(n)$ and $\mathbf{D}(n)$ [11], give the recursive convolution formulation for general dispersive media. Plasma can be considered as a special example.

For unmagnetized plasma, the frequency-domain susceptibility function is given by

$$\chi(\omega) = -\frac{\omega_p^2}{\omega(\omega+i\nu_c)} \tag{11}$$

where ω_p is the angular plasma frequency, and ν_c is the collision frequency. The corresponding time-domain susceptibility function is

$$\chi(t) = \frac{\omega_p^2}{\nu_c}(1-e^{-\nu_c t})U(t). \tag{12}$$

Hence, this medium is a two-pole ($N = 2$) system in (5), with $R_1 = -R_2 = \omega_p^2/\nu_c$, $s_1 = 0$, $s_2 = -\nu_c$.

C. Time-Stepping Equations

With the help of the recursive convolution equations, we can now proceed to solve Maxwell's equations by using the FDTD and PSTD algorithms to discretize the split equations (2) and (3). We obtain the electric field time-stepping equations as follows

$$c_1^{(\eta)}\mathbf{E}^{(\eta)}(n+1) = \frac{\partial}{\partial\eta}\left[\hat{\eta}\times\mathbf{H}\left(n+\frac{1}{2}\right)\right] + c_0^{(\eta)}\mathbf{E}^{(\eta)}(n) - \sigma\omega_\eta\Delta t\mathbf{E}_I^{(\eta)}(n) + \mathbf{\Phi}^{(\eta)}(n) - \mathbf{J}^{(\eta)}(n+\frac{1}{2}) \quad (13)$$

where

$$\mathbf{\Phi}^{(\eta)}(n) = \epsilon_0\sum_{q=1}^{N}\mathrm{Re}\left\{\left[\left(\frac{a_\eta}{\Delta t}-\frac{\omega_\eta}{2}\right)-\left(\frac{a_\eta}{\Delta t}+\frac{\omega_\eta}{2}\right)e^{-s_q\Delta t}\right]\cdot\mathbf{\Psi}_q^{(\eta)}(n)\right\} \quad (14)$$

$$\mathbf{E}_I^{(\eta)}(n) = \mathbf{E}_I^{(\eta)}(n-1) + \tfrac{7}{8}\mathbf{E}^{(\eta)}(n) + \tfrac{1}{8}\mathbf{E}^{(\eta)}(n-1) \quad (15)$$

and

$$c_0^{(\eta)} = \left(\frac{a_\eta}{\Delta t}-\frac{\omega_\eta}{2}\right)\epsilon_0\epsilon_\infty - \frac{q_\eta\sigma}{2} - \left(\frac{a_\eta}{\Delta t}+\frac{\omega_\eta}{2}\right)\epsilon_0\sum_{q=1}^{N}\mathrm{Re}[\hat{\xi}_q(0)] \quad (16)$$

$$c_1^{(\eta)} = \frac{\sigma}{2}[a_\eta + 2s_q\omega_\eta\Delta t] + \left(\frac{a_\eta}{\Delta t}+\frac{\omega_\eta}{2}\right)\cdot\epsilon_0\left\{\epsilon_\infty + \sum_{q=1}^{N}\mathrm{Re}[\hat{\chi}_q(0)-\hat{\xi}_q(0)]\right\}. \quad (17)$$

The magnetic field time-stepping equations remain unchanged for magnetically nondispersive media [16]. Therefore, given the fields at earlier time $t = n\Delta t$, we can find the fields at $t = (n+1)\Delta t$.

D. FDTD and PSTD for Spatial Derivatives

The FDTD method for the spatial derivatives on the right-hand side of (13) remains the same as Yee's scheme [11]. In the PSTD algorithm, the spatial derivatives are approximated by FFT's instead of finite differences. Also, instead of using Yee's grid in the FDTD method, we use a centered grid in which all field components and material parameters are located at the center of each cell. Thus, (13) becomes

$$c_1^{(\eta)}\mathbf{E}^{(\eta)}(n+1) = \mathcal{F}_\eta^{-1}\{ik_\eta\mathcal{F}_\eta[\hat{\eta}\times\mathbf{H}(n+\frac{1}{2})]\} + c_0^{(\eta)}\mathbf{E}^{(\eta)}(n) - \sigma\omega_\eta\Delta t\mathbf{E}_I^{(\eta)}(n) + \mathbf{\Phi}^{(\eta)}(n) - \mathbf{J}^{(\eta)}(n+\frac{1}{2}) \quad (18)$$

and the magnetic field time-stepping equation is given by

$$\left(\frac{a_\eta}{\Delta t}+\frac{\omega_\eta}{2}\right)\mathbf{H}^{(\eta)}\left(n+\frac{1}{2}\right) = -\mathcal{F}_\eta^{-1}\{ik_\eta\mathcal{F}_\eta[\hat{\eta}\times\mathbf{E}(n)]\} - \left(\frac{a_\eta}{\Delta t}-\frac{\omega_\eta}{2}\right)\mathbf{H}^{(\eta)}\left(n+\frac{1}{2}\right) - \mathbf{M}^{(\eta)}(n). \quad (19)$$

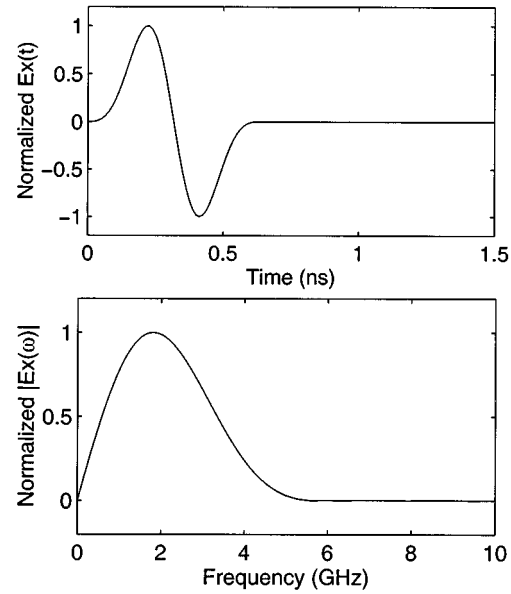

Fig. 1. (a) The source function. (b) Its frequency spectrum.

In the above equations, $\mathcal{F}_\eta$ and $\mathcal{F}_\eta^{-1}$ denote the forward and inverse FFT's in η direction, respectively, and k_η is Fourier variable in the η direction.

III. Numerical Results

In all numerical calculations, the PML equations are used in both the interior region and the matched layers. Ten cells of PMLs are used outside the interior region as the absorbing boundary condition. An electric or magnetic dipole is used as a source. The time function of the source takes two forms: i) the first derivative of the Blackman–Harris window function with central frequency f_c [16] for pulse excitation; and ii) the sinusoidal function for single frequency excitation.

A. Validation

To validate the algorithm, we compare the FDTD and PSTD results with analytical solutions for three test examples. Here the analytical solutions are obtained through an inverse fast Fourier transform (IFFT) of the frequency-domain analytical solutions. In the FDTD and PSTD calculations, the solution region is divided by 64 × 64 × 64 cells. The PSTD results for all test examples have a similar accuracy. Thus, we only show one test example.

First, we consider the transient field produced by an electric or magnetic dipole in infinite homogeneous plasma. The source is located at the origin. The central frequency of source is $f_c = 2.45$ GHz, and the source function and its spectrum are shown in Fig. 1. The plasma parameters are those of Medium I in Table I, and Fig. 2 exhibits the real and imaginary parts of the permittivity. These plots are representative for all other cases in the following. Fig. 3(a) and (b) compare the FDTD results with the analytical solutions for the normalized E_x or H_x produced by an electric or magnetic dipole oriented in the x direction. In this example, the operating frequency band is near the plasma frequency where significant resonance is observed. We refer to this frequency band as the resonance region.

TABLE I
PARAMETERS FOR PLASMA

Medium	ω_p (rad/s)	ν_c (Hz)
I	1.7857×10^{10}	2×10^9
II	3.8489×10^9	2×10^9
III	3.5565×10^{14}	2×10^{13}

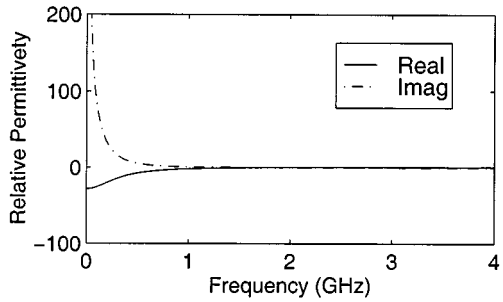

Fig. 2. Complex permittivity of plasma (Medium I).

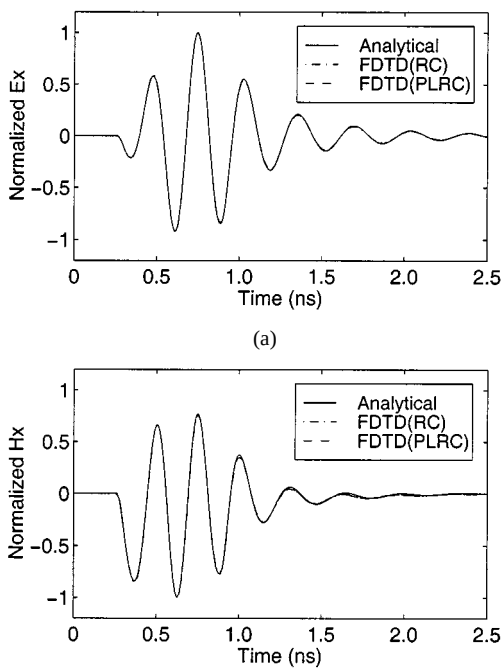

Fig. 3. (a) The E_x field excited by an electric dipole, and (b) H_x field excited by a magnetic dipole in homogeneous Medium I. $f_c = 2.45$ GHz, $\mathbf{r}' = (0, 0, 0)$, $\mathbf{r} = (5, 0, 6.25)$ cm, $\Delta x = \Delta y = \Delta z = 0.3125$ cm, $\Delta t = 1.25$ ps.

Next, we use the same geometrical and excitation model as above, except that Medium I is replaced by Medium II in Table I. In this example, the operating frequency band is now lower than the plasma frequency, which is the most dispersive range of the medium. We refer to this frequency range as the low-frequency region. Fig. 4 shows both the FDTD and analytical results.

The third test example is the transient radiation from an $\hat{x}$-directed electric dipole in an infinite homogeneous plasma (Medium III). The operating frequency band is higher than the plasma frequency, where the dispersion is minimum. This

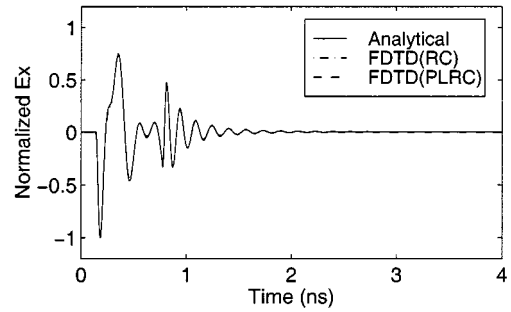

Fig. 4. The E_x field excited by an electric dipole in homogeneous Medium II. $f_c = 2.45$ GHz, $\mathbf{r}' = (0, 0, 0)$, $\mathbf{r} = (2.2, 0, 4.)$ cm, $\Delta x = \Delta y = \Delta z = 0.2$ cm, $\Delta t = 0.5$ ps.

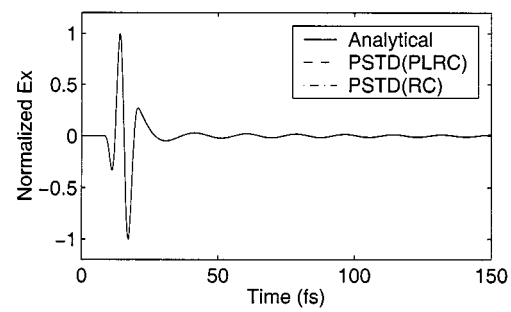

Fig. 5. The E_x field excited by an electric dipole in a homogeneous plasma (Medium III). $f_c = 1.8868 \times 10^{14}$ Hz, $\mathbf{r}' = (0, 0, 0)$, $\mathbf{r} = (0, 0, 3.4069)$ μm, $\Delta x = \Delta y = \Delta z = 0.227\,12$ μm, $\Delta t = 0.025$ fs.

frequency range is referred to as the high-frequency region, where relative small distortion is expected for waves. Fig. 5 compares the PSTD result with analytical solutions for an electric dipole at the central frequency $f_c = 1.8868 \times 10^{14}$ Hz. The discretization is $\Delta x = \Delta y = \Delta z = 0.227\,12$ μm, $\Delta t = 0.05$ fs. (The FDTD result, with $\Delta x = \Delta y = \Delta z = 0.037\,853$ μm, $\Delta t = 0.05$ fs and for exactly the same useful volume, has a comparable accuracy, and is not shown here.) In this example, the FDTD requires a sampling rate six times higher than the PSTD in each direction. Because both methods use ten cells of PML in each side of the boundary, the resulting grid size is therefore, $32 \times 32 \times 64$ for the PSTD, and $92 \times 92 \times 284$ for the FDTD method. Note that the useful volume (excluding PML regions) in both methods is exactly the same, that is $12 \times 12 \times 44 V_0$ (where $V_0 = 0.0117$ μm^3 is the volume of a PSTD unit cell). Also note that Δt (thus, the number of time steps) is chosen the same, so that it satisfies the stability condition and accuracy in both methods. Although the PSTD stability for this case allows a much larger Δt, for an adequate accuracy Δt has to be chosen as small as that in the FDTD method because the temporal derivatives are obtained by finite differences in the PSTD as in the FDTD method. (The accuracy of temporal derivatives in both methods is of second order.) The CPU time for each time step is 101.78 s for the FDTD, and 2.667 s for the PSTD method. Thus, the PSTD method is 38 times faster.

Note that in all examples, excellent agreement is found between the numerical results and the analytical solutions, and the RC and PLRC approaches give about the same accuracy.

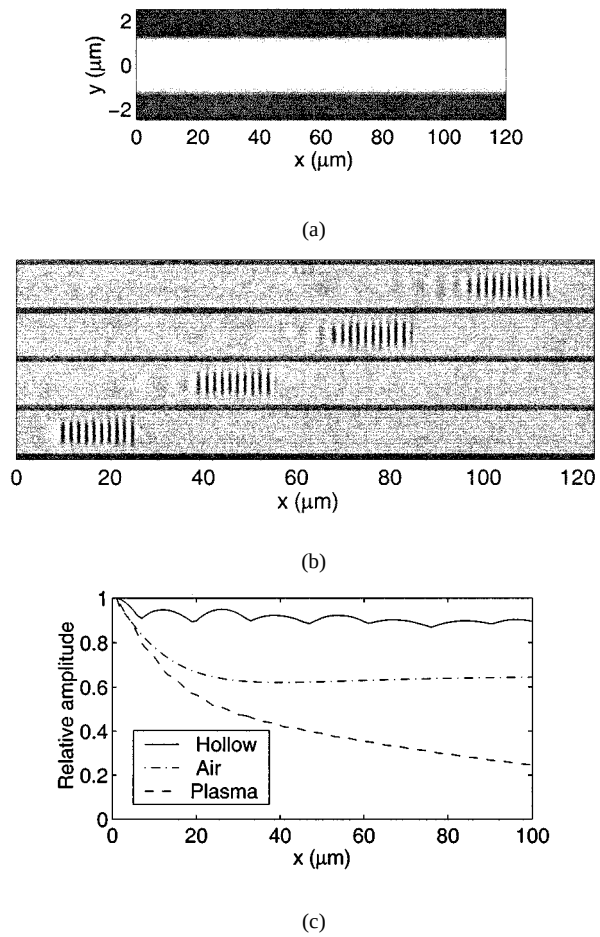

Fig. 6. (a) Geometry of a 2-D plasma hollow with a finite wall thickness. (b) Laser pulse propagation in the hollow. From bottom to top, snapshots at time step $n = 5000,\ 10\,000,\ 15\,000$, and $20\,000$. (c) Comparison of the laser pulse relative amplitude in hollow, air, and homogeneous plasma.

B. Applications

To demonstrate the effectiveness of the algorithms, we consider several novel applications of plasma.

1) Laser Pulse Propagating in Transversely Inhomogeneous Plasma Hollow Channels: One of the important applications of short-pulse laser-plasma interactions is the use of plasma as a particle-accelerating medium [17], [20]. To obtain a long acceleration distance, a new scheme was proposed that uses a hollow channel embedded in a homogeneous underdense plasma to guide short laser pulse [17], [18]. The principle of the plasma channel is similar to those of the optical fiber. The existing analysis of hollow plasma channels uses analytical solution, and is limited to sharp wall of hollow channel [17] or planar layered hollow channels [18].

Here we consider laser propagation in a two-dimensional (2-D) plasma hollow waveguide with a more realistic, finite thickness wall. Fig. 6(a) shows the cross section of the hollow. Air fills in the hollow, and the parameters of plasma are those of Medium III in Table I. Six plasma layers, each of thickness 0.0533 μm, are placed the inner side of the interface of the hollow. The values of ω_p in these transition layers are assumed to be linearly distributed between air and Medium III, but all layers have the same value of ν_c. An $\hat{x}$-directed electric dipole located at the origin of the coordinates excites a 10-period sinusoidal wave at a frequency of 1.8868×10^{14} Hz. In the 2D PSTD calculations, the space and time discretization is $\Delta x = 0.21307\ \mu$m, $\Delta y = 0.05327\ \mu$m, and $\Delta t = 2 \times 10^{-17}$ s. Fig. 6(b) displays the snapshots of the laser wave field in the hollow at four different time steps ($n = 5000,\ 10\,000,\ 15\,000,\ 20\,000$). The laser wave fields are limited within the hollow. They have a slower attenuation than those in homogeneous air and plasma, as shown in Fig. 6(c). In addition, the plasma frequency for underdense plasma is far smaller than laser frequency, and the high frequency response of plasma media only results in the small distortion for incident waveforms. Therefore, the plasma hollow can guide the incident laser to propagate for a relatively long distance.

2) Surface Wave Propagation Along a Plasma Column: At frequencies below the plasma frequency, the plasma permittivity ϵ_p is negative in the absence of losses (i.e., the collision frequency goes to zero). This is a unique characteristic of the plasma medium. Such a medium, when bounded by a dielectric of positive permittivity ϵ_g, provided $|\epsilon_p| > \epsilon_g$, can support surface waves (SWs) which are guided along the boundary surface, their energy flux being concentrated in the vicinity of this surface. The presence of losses will result in the attenuation of the waves both in the direction of propagation, and in the transverse direction [19]. Plasma SWs have found many applications, one of which is SW plasma sources for material processing [20], [21].

The practical SW plasma sources usually use a plasma column of finite length contained in a tube made of fused silica. The previous analysis of properties of SW along a plasma column uses analytical solutions with an infinite column model, for example in [22]. In addition, [23] use the FDTD method [24] to analyze a 2-D SW plasma processing structure in a closed region, where no ABC is needed. Here, we use the FDTD method to simulate a finite plasma column in an open region.

To reduce the staircasing error, a plasma square cylinder model is chosen. The dimension of the cylinder is 2.5 cm $\times$ 2.5 cm $\times$ 28 cm, and the wall thickness of the tube is 0.25 cm. A square cross section is on the x–y plane, and the top part of the cylinder on the x–z plane is shown in Fig. 7(a). The parameters of plasma are $\omega_p = 2\pi \times 6.125 \times 10^9$ rad/s, and $\nu_c = 8 \times 10^8$ Hz, and the relative permittivity of fused silica is 3.78. The outside of cylinder is air. The spatial and temporal cell sizes are $\Delta x = \Delta y = \Delta z = 0.25$ cm, and $\Delta t = 1 \times 10^{-12}$ s, and the number of cells is $56 \times 56 \times 132$. An $\hat{x}$-directed electric dipole with $f_c = 2.45$ GHz is located at the origin of the coordinates. To study the propagation properties, the PML cells are used at the bottom end of the cylinder to truncate the semi-infinite waveguide. The distribution of the electric energy at $f = 2.7$ GHz on the x–z plane and on the straight lines, $y = 0$, $z_i = 2.5i$ ($i = 1, 2, \ldots, 6$) cm, are shown in Fig. 7(b) and (c), respectively. It is obvious that the waves near the surface of the plasma column undergo less attenuation, therefore, the surface waves indeed exist. Furthermore, the numerical results also show that the speed of surface waves is smaller than the speed of light, confirming the slow wave property of plasma SWs.

Note that here we have simulated a square cylinder. For cylindrical structures, one can use these methods in cylindrical coordinates. The implementation of PML, PSTD, and frequency dispersion poses no practical difficulties; indeed elements of these

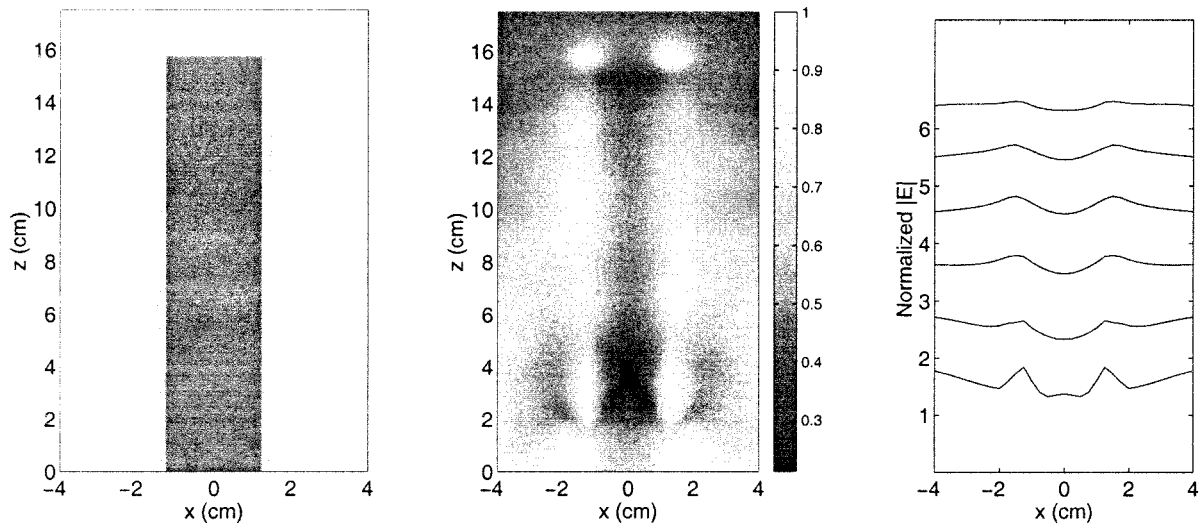

(a) (b) (c)

Fig. 7. Surface wave propagation along a plasma column in a silica tube. (a) The geometry of the plasma column. The distribution of density of electric field at $f = 2.7$ GHz (b) on $y = 0$ plane and (c) along straight lines $y = 0$ cm, $z_i = 2.5i$ ($i = 1, 2, \ldots, 6$) cm.

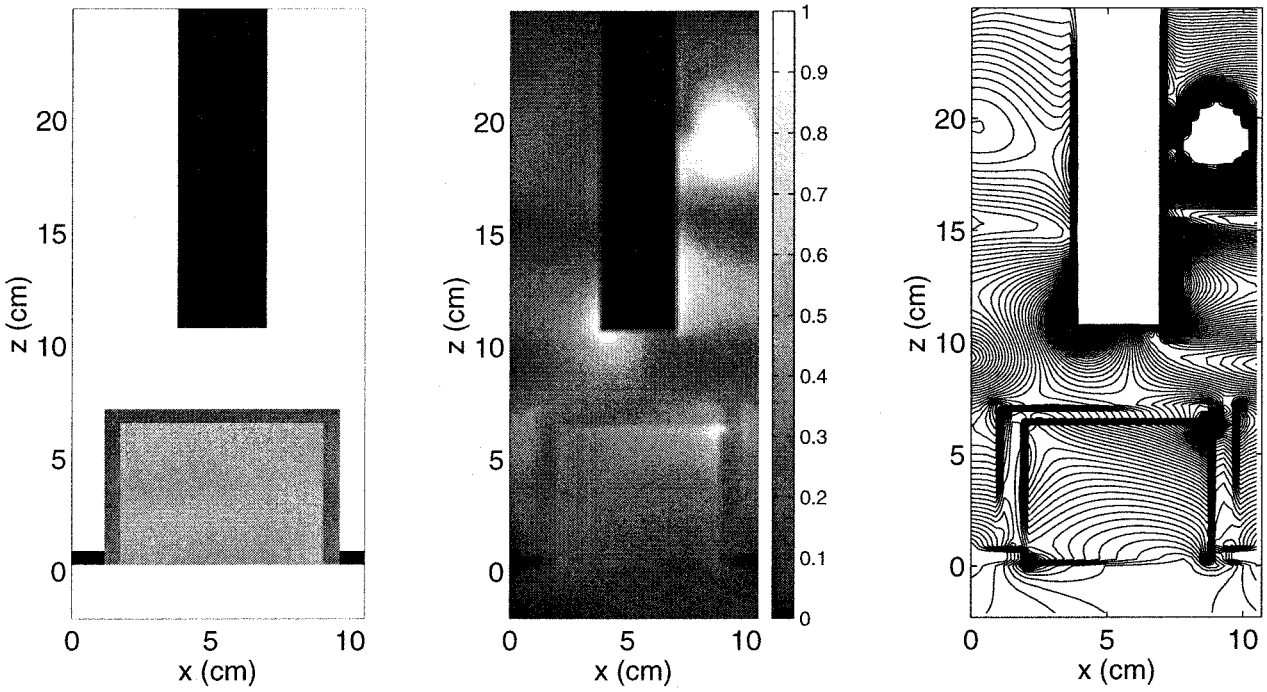

(a) (b) (c)

Fig. 8. (a) The geometry of ECR. The distribution of density of electric field on $y = 0$ plane in (b) the ECR in gray level and (c) in contour plot .

methods can be found in [30]–[32]. An alternative solution is to use a multidomain PSTD algorithm currently under our development.

3) Power Deposition of Electron Cyclotron Esonance (ECR) Plasma Source: The ECR plasma source is a new generation of high-density plasma sources for material processing developed rapidly over the past ten years [23]–[26]. In an ECR source, microwave power is used to excite plasma discharge through ECR heating. The simulation and design of ECR sources require the solution of both electromagnetic field and plasma discharge behavior in a self-consistent manner. As the first step, one needs to solve for the microwave field distribution or power deposition in the region of interest. References [27]–[29] used FDTD to model the ECR source, but did not account for the dispersive effect of plasma when using a single frequency excitation of finite time duration.

In the following, we consider a model of compact ECR plasma source, as depicted in Fig. 8(a). The center conductor, quartz dome, and plasma region are cylinders, but for simplicity the outer conductor is taken as rectangular. The loop antenna is modeled by a magnetic dipole, located at $\mathbf{r}' = (9, 5.4, 19)$ cm. The electric parameters of quartz are $\varepsilon_r = 3.78$, $\mu_r = 1$, and the parameters of plasma are those of the Medium III in Table I. For simplicity, we ignore the effect of the permanent magnets,

as in [28]. In the FDTD simulation, the computational domain is divided into $36 \times 36 \times 100$ cells. Fig. 8(b) and (c) show the distribution of the density of electric field at $f = 2.45$ GHz in ECR source in the forms of gray-level and equal-value contours. Note that the distribution is not symmetrical about the central axis because of the location of the excitation. These visualized results will help the design of the ECR plasma source.

4) Discussions: Finally, we are in position to make a comparison between the FDTD and PSTD method. For large-scale problems the PSTD method has significant advantages over the FDTD method in terms of CPU time and computer memory, as well as in the accuracy of algorithm. To achieve reasonable accuracy, the FDTD algorithm requires more than ten points per minimum wavelength, while the PSTD algorithm allows a near-Nyquist sampling rate. For 3-D problems, this results in a significant saving of computer memory and CPU time. However, if the geometry has subwavelength details or curved boundaries (for example, a meshed human head) which require a small spatial cell size in both FDTD and PSTD methods, the FDTD method may be more advantageous. This is because for 3D problems the CFL stability condition for the FDTD ($\Delta t \leq \Delta x/\sqrt{3}c$) is better than the PSTD method ($\Delta t \leq 2\Delta x/\pi\sqrt{3}c$) (see derivation in [13]), and because Δx has to be small for both methods as required by the geometrical description. In this case, even though the PSTD is applicable, it will be slower than the FDTD method. For example, for the same grid size of $64 \times 64 \times 64$, the CPU time per time step in PSTD is 63% higher than that in FDTD method. We are currently developing a multidomain PSTD method for more general applications.

IV. Conclusion

We present 3-D FDTD and PSTD algorithms with the PML absorbing boundary condition for plasma as a special case of general inhomogeneous, dispersive, conductive media. The algorithms are tested for three typical frequency bands, and an excellent agreement between the FDTD/PSTD results and analytical solutions is obtained for all cases. Several novel applications are demonstrated for laser in a transverse inhomogeneous plasma hollow channel, and the energy deposition in microwave excited SWs and ECR plasma sources for material processing. The numerical results show that the PSTD algorithm is more efficient and accurate than the FDTD algorithm, and is suitable for large-scale problems. The algorithms proposed are ideal for parallel computation, since the same code is shared both in the interior computational region and the outer matched layers. Because of their flexibility and generality, the algorithm and computer program can be used to simulate various electromagnetic waves plasma problems with complex geometry and media constitution, both in time and frequency domains.

Acknowledgment

The authors would like to thank Dr. D. Womble of Sandia National Laboratories, Albequerque, NM, for the suggestions leading to this research. They are grateful to the Klipsch School of Electrical and Computer Engineering, New Mexico State University, Las Cruces, for the use of their HP SPP-2000 Exemplar in the numerical computation. They acknowledge the helpful comments by two reviewers to improve the manuscript.

References

[1] R. J. Luebbers, F. P. Hunsberger, and K. Kunz, "A frequency-dependent finite-difference time-domain formulation for transient propagation in plasma," *IEEE Trans. Antennas Propagat.*, vol. 39, pp. 29–39, Jan. 1991.

[2] R. J. Luebbers, D. Steich, and K. Kunz, "FDTD calculation of scattering from frequency-dependent materials," *IEEE Trans. Antennas Propagat.*, vol. 41, pp. 1249–1257, Sept. 1993.

[3] D. F. Kelley and R. J. Luebbers, "Piecewise linear recursive convolution for dispersive media using FDTD," *IEEE Trans. Antennas Propagat.*, vol. 44, pp. 792–797, June 1996.

[4] J. L. Young, "A full finite difference time domain implementation for radio wave propagation in a plasma," *Radio Sci.*, vol. 29, no. 6, pp. 1513–1522, 1994.

[5] L. J. Nickisch and P. M. Franke, "Finite-difference time-domain solution of Maxwell's equations for the dispersive ionosphere," *IEEE Antennas Propagat. Mag.*, vol. 34, pp. 33–39, Jan. 1992.

[6] S. A. Cummer, "An analysis of new and existing FDTD methods forisotropic cold plasma and a method for improving their accuracy," *IEEE Trans. Antennas Propagat.*, vol. 45, pp. 392–400, Mar. 1997.

[7] D. M. Sullivan, "Exceeding the courant condition with the FDTD method," *IEEE Microwave Guided Wave Lett.*, vol. 6, pp. 289–291, Aug. 1996.

[8] G. Mur, "Absorbing boundary conditions for the finite-difference approximation of the time-domain electromagnetic-field equations," *IEEE Trans. Electromag. Compat.*, vol. EMC-23, pp. 377–382, Aug. 1981.

[9] Z. P. Liao *et al.*, "A transmitting boundary for transient wave analysis," *Science Sinica*, ser. A, vol. 27, pp. 1063–1076, 1984.

[10] J. R. Berenger, "A perfectly matched layer for the absorption of electromagnetic waves," *J. Comp. Phys.*, vol. 114, pp. 185–200, 1994.

[11] G.-X. Fan and Q. H. Liu, "An FDTD algorithm with perfectly matched layers for general dispersive media," *IEEE Trans. Antennas Propagat.*, vol. 48, pp. 637–646, May 2000.

[12] Q. H. Liu and G.-X. Fan, "A frequency-dependent PSTD algorithm for general dispersive media," *IEEE Microwave Guided Wave Lett.*, vol. 9, pp. 51–53, Sept. 1999.

[13] Q. H. Liu, "The PSTD algorithm: A time-domain method requiring only two cells per wavelength," *Microwave Opt. Technol. Lett.*, vol. 15, no. 3, pp. 158–165, 1997.

[14] Q. H. Liu and G. X. Fan, "Simulations of GPR in dispersive media using a frequencydependent PSTD algorithm," *IEEE Trans. Geosci. Remote Sensing*, vol. 37, pp. 2317–2324, Oct. 1999.

[15] W. C. Chew and W. H. Weedon, "A 3D perfectly matched medium from modified Maxwell's equation with stretched coordinates," *Microwave Opt. Tech. Lett.*, vol. 7, no. 13, pp. 599–604, 1994.

[16] Q. H. Liu, "An FDTD algorithm with perfectly matched layers for conductive media," *Microwave Opt. Tech. Lett.*, vol. 14, no. 2, pp. 134–137, 1997.

[17] T. C. Chiou *et al.*, "Laser wake-field acceleration and optical guiding in a hollow plasma channel," *Phys. Plasma*, vol. 2, no. 1, pp. 310–318, 1995.

[18] G. Shvets *et al.*, "Excitation of accelerating wakefields in inhomogeneous plasma," *IEEE Trans. Plasma Sci.*, vol. 24, pp. 351–362, Apr. 1996.

[19] M. Moisan, A. Shivarova, and A. W. Trivelpiece, "Experimental investigations of the propagation of surface waves along a plasma column," *Plasma Phys.*, vol. 11, no. 11, pp. 1331–1400, 1982.

[20] M. Moisan and J. Pelletier, Eds., *Microwave Excited Plasmas*. Amsterdam, The Netherlands: Elsevier, 1992.

[21] Y. M. Aliev *et al.*, "Theory on electromagnetic surface wave propagation in inhomogeneous plasma," *J. Electromag. Waves Appl.*, vol. 9, no. 5-6, pp. 697–733, 1995.

[22] Q. Chen, P. H. Aoyagi, and M. Katsurai, "Numerical analysis of surface wave excitation in a plasma-type nonmagnetized plasma processing device," *IEEE Trans. Plasma Sci.*, vol. 27, pp. 164–170, Feb. 1999.

[23] Q. Chen, M. Katsurai, and P. H. Aoyagi, "An FDTD formulation for dispersive media using a current density," *IEEE Trans. Antennas Propagat.*, vol. 46, pp. 1739–1746, Nov. 1998.

[24] *High Density Plasma Sources*. Park Ridge, NJ: Noyes, 1995.

[25] M. A. Lieberman and A. J. Lichtenberg, *Principles of Plasma Discharges and Materials Processing*. New York: Wiley, 1994.

[26] V. P. Gopinath and T. A. Grotjohn, "Three-dimensional electromagnetic PIC model of a compact ECR plasma source," *IEEE Trans. Plasma Sci.*, vol. 23, pp. 602–608, Aug. 1995.

[27] J. Asmussen *et al.*, "The design and application of electron cyclotron resonance discharges," *IEEE Trans. Plasma Sci.*, vol. 25, pp. 1196–1221, Dec. 1997.

[28] T. A. Grotjohn, "Numerical modeling of a compact ECR ion source," *Rev. Sci. Instrum.*, vol. 63, no. 4, pp. 2535–2537, 1992.

[29] T. A. Grotjohn *et al.*, "Modeling the electromagnetic excitation of a compact ECR ion/free radical source," *Rev. Sci. Instrum.*, vol. 65, no. 5, pp. 1761–1765, 1994.

[30] E. F. Jaeger *et al.*, "Power deposition in highdensity inductively coupled plasma tools for semiconductor processing," *Phys. Plasmas*, vol. 2, no. 6, pp. 2597–2604, 1994.

[31] J. He and Q. H. Liu, "A nonuniform cylindrical FDTD algorithm with improved PML and quasi-PML absorbing boundary conditions," *IEEE Trans. Geosci. Remote Sensing*, vol. 37, pp. 1066–1072, Mar. 1999.

[32] Q. H. Liu and J. Q. He, "A PSTD algorithm in cylindrical coordinates," presented at the 14th Annu. Review of Progress in Applied Computational Electromagnetics, Monterey, CA, Mar. 1998.

[33] F. L. Teixeira and W. C. Chew, "Finite-difference computation of transient electromagnetic waves for cylindrical geometries in complex media," *IEEE Trans. Geosci. Remote Sensing*, vol. 38, pp. 1530–1543, July 2000.

Guo-Xin Fan (M'97) received the Ph.D. degree in electrical engineering from Tsinghus University, Bejing, China, in 1995.

From 1985 to 1990, he was a Research Engineer and the Head of a research group on the theory and techniques of subsurface detection at the China Research Institute of Radiowave Propagation, Xinxiang, China. He was in charge of the development of the first practical ground-penetrating radar in China. From September 1995 to August 1997, he was a Postdoctoral Research Fellow in the Electromagnetics Laboratory, Department of Electrical and Computer Engineering, University of Illinois at Urbana–Champaign. From August 1997 to September 1999, he was a Postdoctoral Research Associate in the Electromagnetics Laboratory, Klipsch School of Electrical and Computer Engineering, New Mexico State University, Las Cruces. Since October 1999, he has been a Research Associate in the Department of Electrical and Computer Engineering, Duke University, Durham, NC. His research interests include computational electromagnetics, electromagnetic scattering, slotted-waveguide array antenna, subsurface target detection, and the development of ground-penetrating radar.

Dr. Fan was the first winner of the Science and Technology Progress Award of the Ministry of Electronics Industry of China in 1991.

Qing Huo Liu (S'88–M'89–SM'94) received the Ph.D degree in electrical engineering from the University of Illinois at Urbana–Champaign in 1989.

He was with the Electromagnetics Laboratory, University of Illinois at Urbana–Champaign, as a Research Assistant from September 1986 to December 1988 and as a Postdoctoral Research Associate from January 1989 to February 1990. He was a Research Scientist and Program Leader at Schlumberger-Doll Research, Ridgefield, CT, from 1990 to 1995. From October 1995 to May 1999, he was with New Mexico State University, Las Cruces. He has been an Associate Professor of Electrical Engineering at Duke University, Durham, NC, since June 1999. His research interests include computational electromagnetics and acoustics and their applications, wave propagation in inhomogeneous media, geophysical subsurface sensing, and inverse problems. He has authored more than 150 papers published in refereed journals and conference proceedings.

Dr. Liu is a member of Phi Kappa Phi, Tau Beta Pi, SEG, and a full member of the U.S. National Committee of URSI Commissions B and F. Currently, he serves as an Associate Editor for the IEEE TRANSACTIONS ON GEOSCIENCE AND REMOTE SENSING, for which he also served as a Guest Editor for a special issue on computational methods. He received a Presidential Early Career Award for Scientist and Engineers from the National Science and Technology Council, an Early Career Research Award from the Environmental Protection Agency in 1996, and a CAREER Award from the National Science Foundation in 1997.

Scott A. Hutchinson (S'91–M'92) received the B.S.E.E, M.S.E.E., and Ph.D. degrees from New Mexico State Univserity, Las Cruces, in 1989, 1990, and 1993, respectively.

Since 1992, he has been with the Parallel Computational Sciences Department, Sandia National Laboratories, Albuquerque, NM. His research interests include computational electromagnetics, computational plasmas, bioelectromagnetics, parallel finite-element methods, and the parallel solution of linear systems. He is currently a Principle Member of the Technical Staff, Sandia National Laboratories, where he is working on developing parallel circuit and device modeling capabilities.

Dr. Hutchinson was a member of two finalist teams for the Gordon Bell High Performance Computing Competitions, and won the R&D 100 Award in 1997 for his work on the Aztec parallel sparse-matrix solver library.